

# Design and Investigation of TiO<sub>2</sub>-SiO<sub>2</sub> Thin Films on AISI 316L Stainless Steel for Tribological Properties and Corrosion Protection

B. Shayegh Boroujeni<sup>a,\*</sup>

<sup>a</sup> Department of Engineering, Shahrekord University, Shahrekord, Iran.

---

## ARTICLE INFO

### Article history:

Received 09 August 2015

Accepted 16 August 2015

Available online 30 September 2015

### Keywords:

TiO<sub>2</sub>-SiO<sub>2</sub> Nanocomposite  
Films

Sol-gel

Depth-sensing Indentation  
Technique

Photocathodic Protection Effect

## ABSTRACT

The TiO<sub>2</sub>-SiO<sub>2</sub> thin films were deposited on the AISI 316L stainless steel via the sol-gel method. Then, the effect of the added amount of SiO<sub>2</sub> on the structure, morphology and mechanical properties of the films and corrosion behavior of the AISI 316L stainless steel substrate were investigated. By using X-ray diffraction, field-emission scanning electron microscopy, atomic force microscopy, depth-sensing indentation technique supporting micro-scratch mode and potentiodynamic polarization test. It was observed that the appropriate amount of SiO<sub>2</sub> addition to the TiO<sub>2</sub> film not only decreased the particle size of the TiO<sub>2</sub>-SiO<sub>2</sub> crystal but also could help to improve the surface quality. Mechanical and tribological properties of the films were found to be improved in the range of 10–15% mol of SiO<sub>2</sub> addition compared with the pure TiO<sub>2</sub>. The minimum root mean square value was obtained from the film with a silica content of 10% mol. In addition, the corrosion behavior of the AISI 316L stainless steel was improved by adding 15% mol of SiO<sub>2</sub>. Under the UV illumination conditions, photo-generated electrons accumulated in this film could perfectly protect the substrate photocathodically.

---

## 1. Introduction

Ceramic coatings on metal substrate have been essentially studied for their oxidation resistance and their applications for corrosion protection [1-4]. TiO<sub>2</sub>-SiO<sub>2</sub>, as a ceramic coating, has already attracted much attention in recent years not only for its possible applications in corrosion protection of the carbon steel [5-7] but also for its uses in photocatalysis [8-10] and self-cleaning [11-12]. In addition, TiO<sub>2</sub>-SiO<sub>2</sub> nano-composites can be used as very interesting glass materials with ultra-low thermal expansion coefficients and high

refractive indices [13-14]. Such advanced materials are naturally expected to include the properties of both phases including corrosion protection, high thermal stability and excellent mechanical strength as the properties of SiO<sub>2</sub> and chemical stability and higher coefficient of thermal expansion as the properties of TiO<sub>2</sub>. Furthermore, the TiO<sub>2</sub>-SiO<sub>2</sub> mixed oxides extend their uses through the production of new catalytic active sites due to the interaction of TiO<sub>2</sub> with SiO<sub>2</sub> [15]. Austenitic stainless steel, especially AISI 316L, has been extensively and

---

Corresponding author:

E-mail address: b.shayegh@eng.sku.ac.ir (Behrooz Shayegh Boroujeni).

used in the production of medical devices body implants owing to its good corrosion resistance and biocompatibility [16-17]. However, very few efforts have been made to apply  $\text{TiO}_2\text{-SiO}_2$  to metallic alloys especially to the family of stainless steel for tribological and anti-corrosion applications. In our previous work [12], we investigated the photocatalytic activity of the  $\text{TiO}_2\text{-SiO}_2$  thin films coated on AISI 316L. It was observed that the photocatalytic activity, the super-hydrophilicity and the self-cleaning properties of the films could be improved by adding  $\text{SiO}_2$  to  $\text{TiO}_2$ . As a semiconductor under normal conditions,  $\text{TiO}_2$  absorbs light with energy equal to or greater than its band gap energy resulting in excited charge carriers: an electron,  $e^-$ , and a hole,  $h^+$ . The  $\text{SiO}_2$  addition to the  $\text{TiO}_2$  matrix increases its band gap from 3.2 to 4.5 eV [18]. As pointed out by Lassaletta et al. [19-20], the increase in the band-gap energy could be attributed to a combination of the quantum-size effect and the interface interaction due to the support effect with the support effect probably being the most important parameter. The oxidizing potential of the photo-generated holes ( $h^+$ ) and the reducing potential of the photo-generated electrons ( $e^-$ ) will increase as band-gap is increased [18]. As a result, the addition of  $\text{SiO}_2$  to  $\text{TiO}_2$  can improve its photocatalytic activity and increase its photo-generated electrons. On the other hand, it is well known that long thermal exposure of austenitic stainless steels to high temperatures (e.g. 700-850°C) can affect the mechanical properties of the film and the corrosion behavior of the

stainless steel. In the present work, corrosion resistance of the 316L stainless steels and the tribological and mechanical properties of the films have been studied by applying the  $\text{TiO}_2\text{-SiO}_2$  coatings on the stainless steel surface. The present paper explains the process, which includes the deposition of the  $\text{TiO}_2\text{-SiO}_2$  coatings with different compositions through the sol-gel method and subsequent sintering heat treatment of the coated AISI 316L stainless steel to produce a hybrid coating with good tribological and anti-corrosion properties.

## 2. Materials and methods

### 2.1. Preparation of thin films

The detailed preparation procedures for the thin films can be found in the literature [12]. An  $\text{SiO}_2$  polymeric sol was prepared by diluting 1 mol of tetraethoxysilane (TEOS) in 2.68 ml ethanol, deionized water, and nitric acid ( $\text{HNO}_3$ ). TEOS concentration in the concentrated sol was 2.35 M with a molar ratio  $\text{H}_2\text{O}/\text{TEOS}$  of 2.2, and a pH of 3.5. This solution was kept at 60°C for 2 days before use. Then 1 mol of tetrakisopropylorthotitanate (TIPT) was dissolved in the solutions containing deionized water and different amounts of ethanol with the  $\text{H}_2\text{O}/\text{TIPT}$  molar ratio of 0.8 used as TIPT precursor solution. Nitric acid ( $\text{HNO}_3$ ) was used for adjusting the pH to 2.5. Then TEOS and various amounts of TIPT precursor solution were mixed to obtain the concentrations listed in Table 1.

**Table 1.** Quantities (mol) of the products used for making the final solution used for thin film preparation

	%mol $\text{SiO}_2$ in composite					
	0	5	10	15	20	25
TEOS	0	0.5	0.1	0.15	0.2	0.25
TTIP	1	0.95	0.9	0.85	0.8	0.75
$\text{H}_2\text{O}$	0.8	0.87	0.94	1.01	1.08	1.15
EtOH	15.9	15.25	14.59	13.93	13.26	12.6

The concentration of alkoxides (TIPT + TEOS) was fixed at 0.8 M in ethanol. Before the

application, the mixed sol was stirred for 2 h. The surfaces of the AISI 316L austenitic

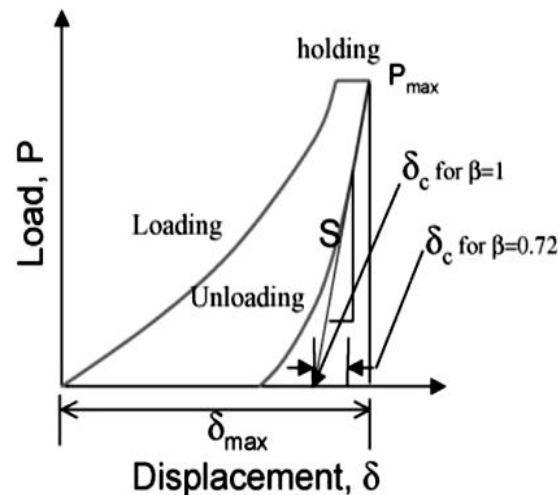


Fig. 1. Schematic illustration of the load-displacement curve for an indentation

stainless steel substrate were prepared by manual grinding for different grades of SiC papers (600-1500) to produce a mirror surface. The coatings were prepared by dipping the substrates into the solution, followed by drying and then heat treating in a programmable furnace. The withdrawal rate used for preparing the films was 5 cm/min. The temperature was slowly increased (3°C /min) to 750°C and was kept at this temperature for 1 h. The film thickness was increased by repeated dipping, drying and heat-treating cycles. For all the samples three dipping cycles were repeated. The average thickness of the films was 400 nm.

## 2. 2. Microstructure characterization

The crystal structure of the TiO<sub>2</sub>-SiO<sub>2</sub> films was studied by X-ray diffractometer (Philips PW-3040, 40kV and 30mA) using monochromatized Cu K $\alpha$  radiation ( $\lambda = 0.1506$  nm). The XRD spectra of the films were recorded by scanning  $2\theta$  at the range of 10–90°. The Scherrer equation was used for determining the crystallite size of the films.

## 2. 3. Morphological characterization

Field-emission scanning electron microscopy (FE-SEM, Hitachi 4160, 25kV) and atomic force microscopy (AFM) were used to examine the surface morphology and grain structure of the coatings.

## 2. 4. Mechanical properties characterization

The hardness and elastic modulus of the coatings were evaluated by depth-sensing indentation, a relatively new technique, which has been recently used to investigate the mechanical properties of the thin films. In a depth-sensing indentation test, a diamond tip is indented into the surface of the films and then the corresponding force-displacement curve, which is usually composed of loading, holding, and unloading segments, is traced as Fig.1. In Fig. 1, S is the contact stiffness between the tip and the sample and is determined as the slope of the upper portion of the unloading curve,  $\delta_c$  is the contact depth, and  $\delta_{max}$  is the maximum depth. Generally, the modified Oliver and Pharr's method [21] is used to analyze the indentation force-displacement curve and to calibrate the machine compliance and the indenter tip area function.

Based on this standard analysis, the reduced modulus ( $E_r$ ) is related to S according to the following relationship:

$$E_r = S / 2\sqrt{\pi / A} \quad [1]$$

Where A is the contact area between the tip and coating. Then, the coating modulus ( $E_s$ ) can be calculated from  $E_r$  by equation (2):

$$1 / E_r = (1 - \nu_s^2) / E_s + (1 - \nu_i^2) / E_i \quad [2]$$

Where  $\nu$  is the Poisson ratio, and subscripts s and i refer to sample and indenter, respectively. The hardness (H) of a sample is defined as:

$$H = P_{max} / A \quad [3]$$

Where  $P_{max}$  is the peak indentation load.

The micro-scratch mode of the Nanotest machine using a Berkovich diamond indenter was adopted to determine the adhesion strength of the coating to the substrate. The test involved drawing the indenter over the coating surface at a constant traveling speed and at a continuously increasing load.

## 2. 5. Electrochemical behavior characterization

The corrosion behavior of the specimens was tested in an electrolyte of 3% wt NaCl solution using an Auto lab PGSTAT 30 Electrochemical Measurement System. The electrochemical corrosion test was carried out in a flat cell with the specimen-exposed area of 1 cm<sup>2</sup>. The flat cell included a stainless steel auxiliary electrode, a saturated calomel reference electrode (SCE) and the specimens as working electrodes. The scans were carried out at a rate of 0.1 mV/ sec from - 0.25 V to +0.25 V relative to the open-circuit potential. The TiO<sub>2</sub>-SiO<sub>2</sub> coated AISI 316L stainless steel samples were placed in darkness before measurements.

A 20 W black light bulb was used as a UV light source.

## 3. Results and discussion

### 3. 1. Microstructure of the films

Fig. 2 shows the XRD patterns of silica-embedded titania films that were heat-treated at 750 °C, with an inset showing the crystallite size changes of anatase phase in these films. As is evident in Fig. 2, in the XRD pattern of pure both anatase ( $2\theta = 25.2^\circ$ ) and rutile ( $2\theta = 27.5^\circ$ ) phases existed in the structure of the film. The rutile phase disappeared when the silica percentage exceeded 10% mol. The peaks gradually broadened as SiO<sub>2</sub> was added. Therefore, the crystallite size of anatase decreased when silica content of the films increased.

The anatase phase has a tetragonal unit cell and the lattice parameters (a, c) which can be determined from the peak positions (004) and (200) by the relations  $a = b = 2 \times d_{200}$  and  $c = 4 \times d_{400}$ . The lattice parameters calculated for the films are shown in Table 2.

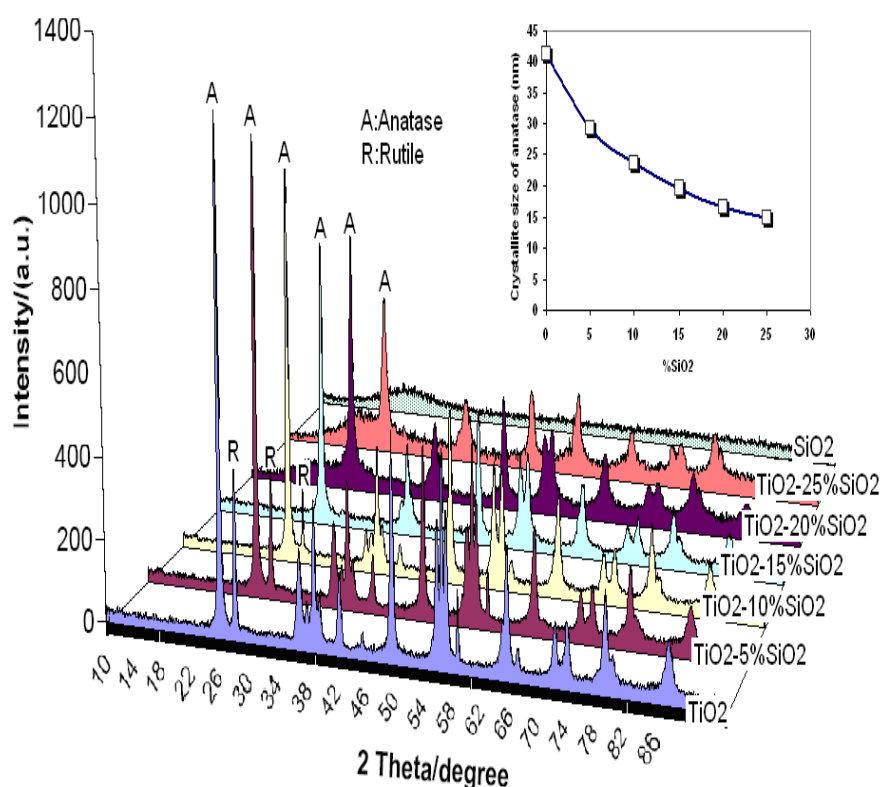
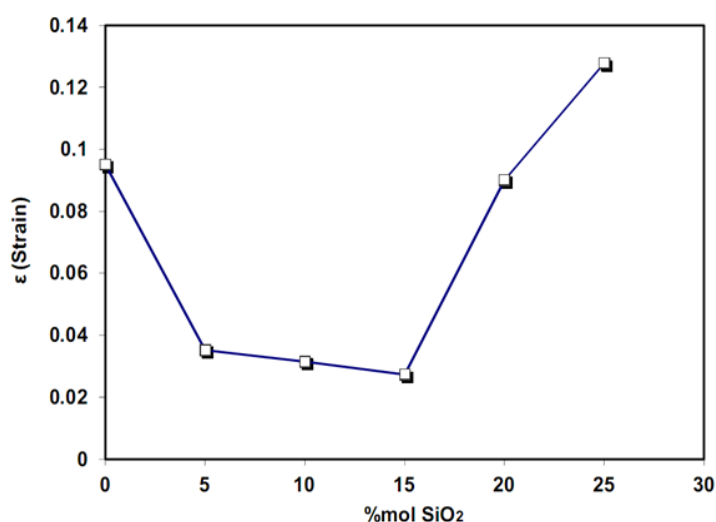


Fig. 2. XRD patterns of silica-embedded titania films heat-treated at 750°C. Inset shows effect of the silica content on the crystallite size of anatase

**Table 2.** The lattice parameters calculated for the films

Silica content (% mol)	Lattice parameter (a)(°A)	Lattice parameter (c)(°A)	Ratio of lattice constants(c/a)
0	3.7822	9.5007	2.5121
5	3.7811	9.4901	2.5099
10	3.7852	9.4878	2.5066
15	3.7851	9.4884	2.5068
20	3.7912	9.4655	2.4967
25	3.7958	9.4574	2.4915

**Fig. 3.** The variation of the residual strain with the films silica content

Among these data, the lattice parameters calculated for the films containing 10-15% mol SiO<sub>2</sub> were close to the reported bulk values of the anatase phase (a = 3.7842 °A, c = 9.5146 °A) [22]. It was observed that the lattice constant a decreased with the silica percentage, whereas the lattice constant c increased. It can also be seen from Table 2 that all films were under tensile strain since the ratio of the lattice constants c/a was lower than the c/a ratio (2.5142) of the stress free TiO<sub>2</sub> [22]. Equation (4) shows the relationship between the FWHM (β) and residual strain [24]:

$$\beta \cdot \cos \theta = k\lambda / D + 4\epsilon \cdot \sin \theta \quad [4]$$

The strain ε was estimated from the slope of the plot β Cosθ versus Sinθ. The variation of the strain with the films silica content is shown in Fig. 3.

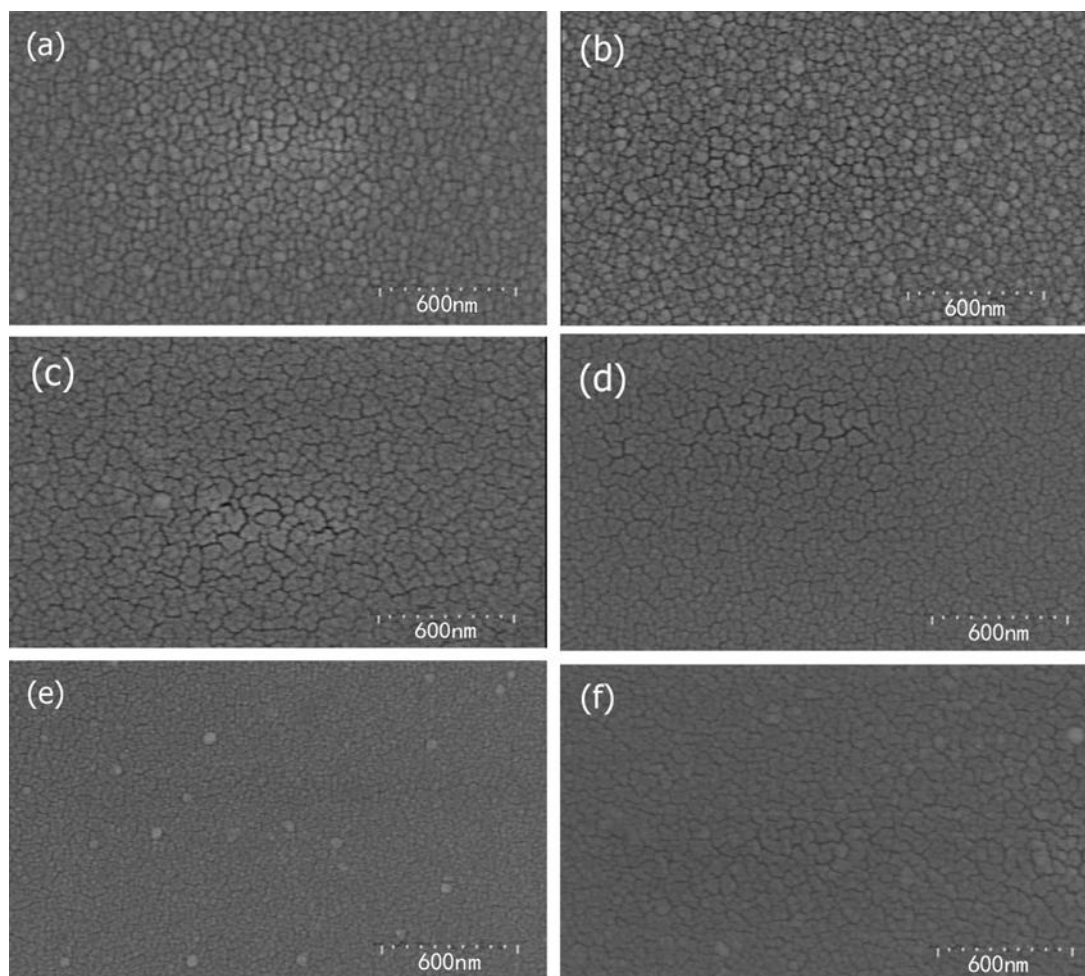
It is clear that when the films silica content increased to 15% mol, the strain initially decreased and then increased considerably. The decrease in strain implies a decrease in the lattice imperfections. Therefore, it is expected that adding 10-15% mol of SiO<sub>2</sub> into TiO<sub>2</sub> could improve some of its properties such as photocatalytic activity. This has been reported in some previous relevant literature [12, 24-25]. Further addition of silica caused the residual strain to increase.

### 3. 2. Morphological studies

The SEM micrographs of the surface of silica-embedded titania films heat-treated at 750°C are shown in Fig. 4. The quality of the thin films prepared on the substrate was uniform and homogeneous. The films exhibited a granular structure and were composed of

monodispersed uniformly distributed globular particles. It can be clearly seen that the particle size of the  $\text{TiO}_2$ - $\text{SiO}_2$  coatings considerably varied with the presence and the amount of  $\text{SiO}_2$ . In the case of the thin film which consisted of only  $\text{TiO}_2$  (Fig. 4a), the particle size of the  $\text{TiO}_2$  crystal was about 50-60 nm. However, the particle size of the  $\text{TiO}_2$ - $\text{SiO}_2$  crystal decreased as the silica percentage in the thin films increased. For example, the particle size of  $\text{TiO}_2$ - $\text{SiO}_2$  crystal was as small as about

30 nm in the film in which 15% mol  $\text{SiO}_2$  was added (Fig. 4d). It seems that  $\text{SiO}_2$  prevented the contact between  $\text{TiO}_2$  particles and, as a consequence, obviously small particles were observed as compared to the pure  $\text{TiO}_2$  coating. In addition, the surface of the films became smoother with the increase in the silica content of the films. By adding up to 15% mol of  $\text{SiO}_2$ , the films turned to a more agglomerated state so that the surface of these films became rougher.



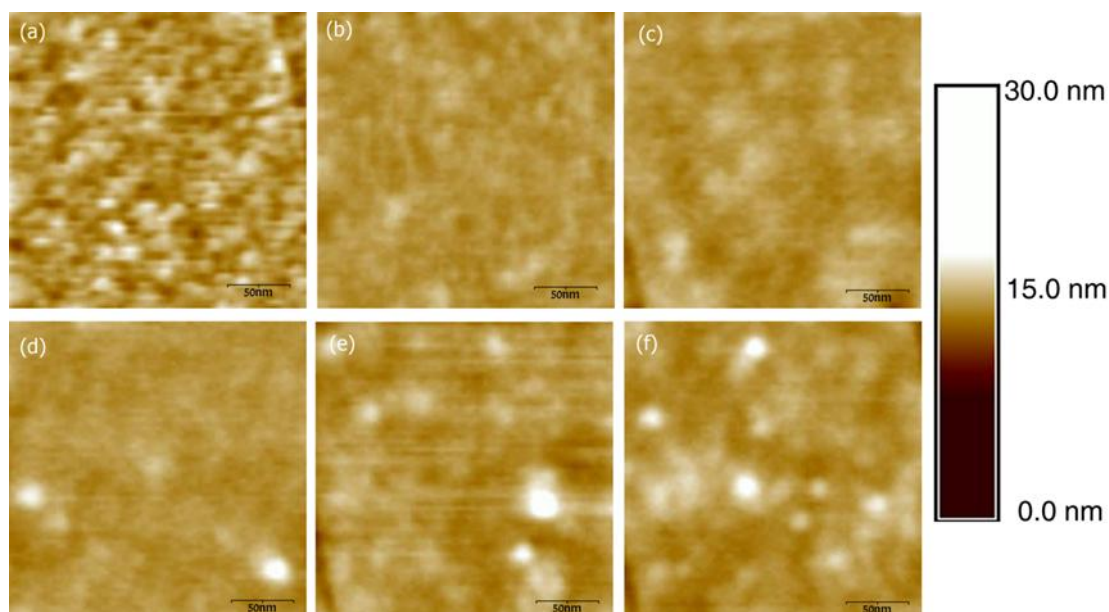
**Fig. 4.** The SEM micrographs of the surface of silica-embedded titania films heat-treated at 750°C: (a):  $\text{TiO}_2$ , (b):  $\text{TiO}_2$ -5% mol  $\text{SiO}_2$ , (c):  $\text{TiO}_2$ -10% mol  $\text{SiO}_2$ , (d):  $\text{TiO}_2$ -15% mol  $\text{SiO}_2$ , (e):  $\text{TiO}_2$ -20% mol  $\text{SiO}_2$ , (f):  $\text{TiO}_2$ -25% mol  $\text{SiO}_2$

Fig. 5 shows the AFM images of the films with a granular structure consisting of interconnected grain particles fused together. It can be seen that the surface of the films became smoother with the addition of  $\text{SiO}_2$  into  $\text{TiO}_2$

which is in agreement with the results of the SEM studies. Although the morphologies of the silica-containing films were similar, their factors of surface roughness, represented by a root mean square (RMS), were different. The

dependence of the RMS roughness of the films on the silica content is shown in Fig. 6. As is evident in Fig.6, the minimum RMS, 0.916, belonged to the  $\text{TiO}_2\text{-SiO}_2$  nanocomposite film that contained 10%mol of silica. The RMS of the surface of the films increased with the addition of up to 10% mol of  $\text{SiO}_2$ , indicating

that the addition of suitable amount of  $\text{SiO}_2$  to the  $\text{TiO}_2$  film could help to improve the surface quality. Some literature works aimed at investigating the hydrophilic properties of the  $\text{TiO}_2\text{-SiO}_2$  film confirmed that the addition of 10-15% mol of  $\text{SiO}_2$  improves the surface superhydrophilicity [12, 26].



**Fig. 5.** AFM images of the surface of silica-embedded titania films heat-treated at 750°C, (a), (b):  $\text{TiO}_2\text{-5%mol SiO}_2$ , (c):  $\text{TiO}_2\text{-10%mol SiO}_2$ , (d):  $\text{TiO}_2\text{-15%mol SiO}_2$ , (e):  $\text{TiO}_2\text{-20%mol SiO}_2$ , (f):  $\text{TiO}_2\text{-25%mol SiO}_2$

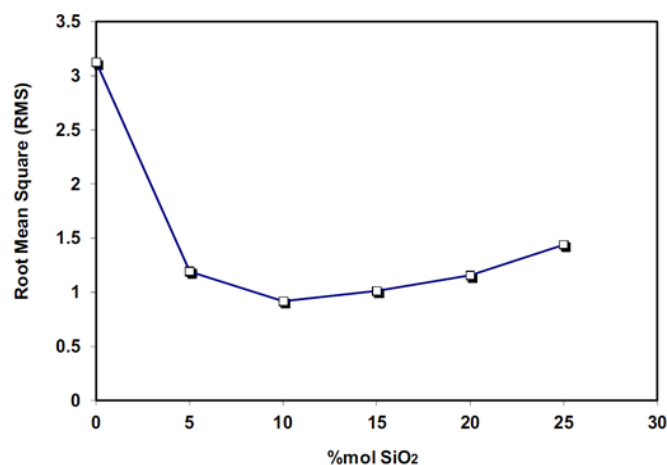


**Fig. 6.** The dependence of the RMS roughness of the films on the silica content

### 3. 3. Mechanical properties

Fig. 7a shows the hardness values determined by nanoindentation of the coatings as a function of the silica percentage of the coatings.

According to Fig. 7a, the hardness of the composite coatings decreased as the  $\text{SiO}_2$  content increased up to 5% mol and, consequently, it substantially enhanced the

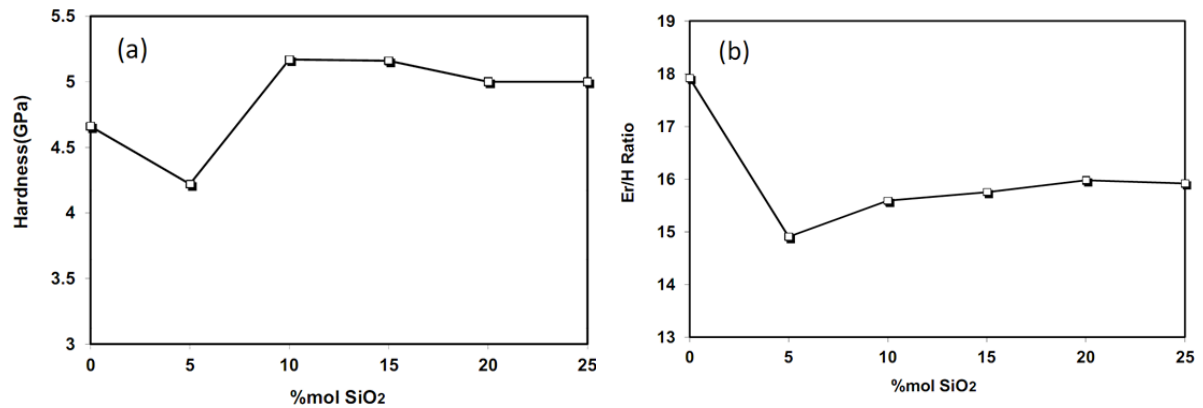


Fig. 7. (a): The hardness values and (b): the  $E_r/H$  ratio of the films as a function of the silica percentage of the coatings

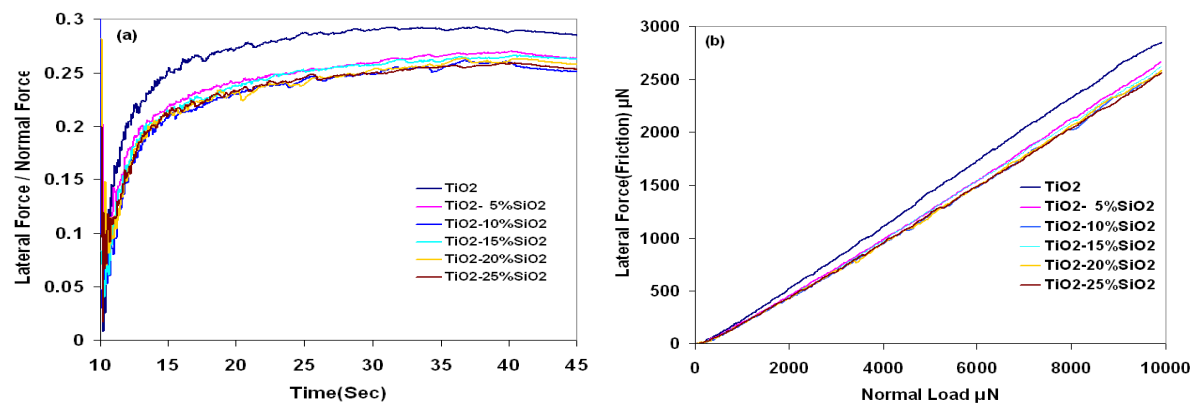


Fig. 8. (a): Changes in the friction coefficient (LF/NF) of the TiO<sub>2</sub>- SiO<sub>2</sub> films containing 0-25% mol of SiO<sub>2</sub> vs. time, (b): comparison of the friction force vs. the load curves measured during the microscratch test of the specimens

hardness of the composite coatings. The maximum hardness of TiO<sub>2</sub>-SiO<sub>2</sub>, ~ 5.2 GPa, belonged to the film which contained 10% mol of silica. In the case of exceeding 10% mol of SiO<sub>2</sub>, the coating hardness appeared to slightly drop and then remained constant.

In Fig. 7b, the ratio of the measured reduced modulus to hardness  $E_r/H$  for each specimen is plotted against the silica content of the films. The  $E_r/H$  ratio is a criterion of the plastic index of the materials, and a small ratio supports elastic deformation during contact motion and is therefore beneficial for enhancing the tribological performance of the material [27-28]. According to Fig. 7b, adding silica into TiO<sub>2</sub> reduced the  $E_r/H$  ratio of the films and therefore it is expected to reveal much enhanced tribological performance.

Changes in the friction coefficient (LF/NF) of the TiO<sub>2</sub>-SiO<sub>2</sub> films containing 0-25% mol of SiO<sub>2</sub> vs. time are depicted in Fig. 8a. As can be seen, the pure TiO<sub>2</sub> film had the maximum friction coefficient, i.e. ~ 0.3. The addition of SiO<sub>2</sub> resulted in the loss of friction coefficient, so that this value would be ~ 0.25 for the films containing 20-25% mol of silica.

Fig. 8b compares the friction force vs. the load curves measured during the micro-scratch test of the specimens. It can be seen that the friction force measured from the Nano composite coatings was much lower than that of the pure TiO<sub>2</sub> coating across the load range, demonstrating the improved frictional properties of the coatings. It is worth noting that these results are in agreement with the AFM and SEM investigations and the obtained RMS values. On the other hand, the adhesive

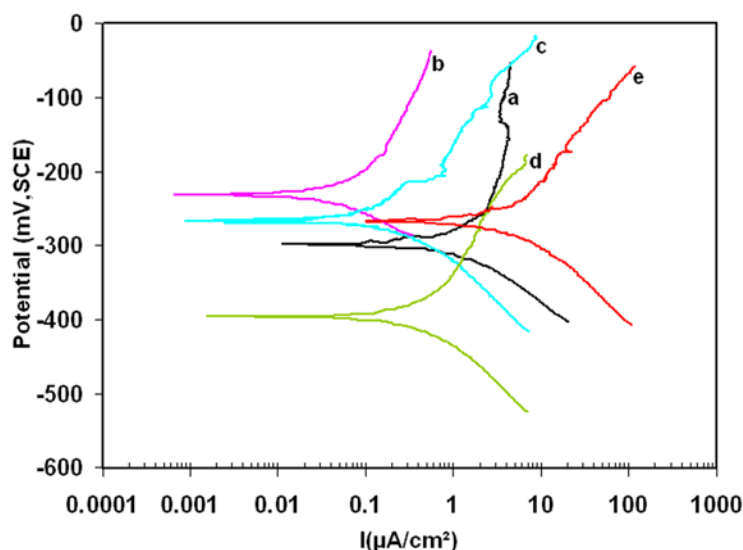


**Fig. 9.** The potentiodynamic polarization curves for: (a): 316L stainless steel, (b): TiO<sub>2</sub>, (c): TiO<sub>2</sub>-5% mol SiO<sub>2</sub>, (d): TiO<sub>2</sub>-15% mol SiO<sub>2</sub>, (e): TiO<sub>2</sub>-25% mol SiO<sub>2</sub> in 3% wt NaCl solutions

strength of the coating to the substrate remarkably increased after the addition of SiO<sub>2</sub> as the coating did not show adhesive failure even for loads up to 10000 μN applied in the test. The adhesion enhancement could be attributed to the interdiffused zone between the TiO<sub>2</sub>-SiO<sub>2</sub> coatings and the stainless steel substrate as the interfacial region is expected to play an important role in the enhancement of the adhesive strength [29-30].

### 3. 4. Corrosion behavior of the coatings

The potentiodynamic polarization curves of the stainless steel substrate and the TiO<sub>2</sub> coatings containing 0, 5, 15 and 25% mol of SiO<sub>2</sub> in 3% wt NaCl solutions are shown in Fig. 9.

The comparison of the electrochemical behaviors of the uncoated substrate curve (a) and the pure TiO<sub>2</sub> film curve (b) indicated that the obtained potential values from the pure TiO<sub>2</sub> film revealed nobler values than those from AISI 316L. So, the stainless substrate will be corroded and pitted if the coating cracks due to the expansion coefficient difference between the stainless steel substrate and the coating. After adding up to 15% mol of SiO<sub>2</sub>, the corresponding curves shifted toward more negative values (c, d) and then the potentials increased to nobler values (e). Among these potentiodynamic polarization curves, the electrochemical behavior of the TiO<sub>2</sub>-SiO<sub>2</sub> film

which contained 15% mol of SiO<sub>2</sub> was different from the others. The corrosion potential of the stainless steel 316L was nobler than the open circuit potential (OCP) of TiO<sub>2</sub>-15% mol SiO<sub>2</sub> film. As a result, the TiO<sub>2</sub>-15% mol SiO<sub>2</sub> film was polarized as an anode. This behavior was similar to that of sacrificial anodes such as zinc in cathodic protection systems for metals. Unlike sacrificial anodes in corrosion system, this film could theoretically act as a non-sacrificial anode because the anodic reaction of this coating (d) was not passivation or the decomposition of the film itself; rather, it was the oxidation of water (H<sub>2</sub>O) and/or adsorbed organic species by the photo-generated holes in the valence band of the TiO<sub>2</sub>-SiO<sub>2</sub> film which can be called photocathodic protection effect of the TiO<sub>2</sub> family semiconductor. As noted before, TiO<sub>2</sub> as a semiconductor under normal conditions absorbs light and produces photo-generated electrons and holes. The photo-generated holes react with water to produce hydroxyl (OH<sup>-</sup>) radicals. So, hydroxyl ions act as hole traps that prevent electron-hole recombination. The increase in surface hydroxyl group can improve the photocatalytic activity of the films. It is well known that a surface with improved acidity can react with water to produce hydroxyl (OH<sup>-</sup>) radicals. It is shown that many binary metal oxides such as the TiO<sub>2</sub>-SiO<sub>2</sub> composites show highly acidic

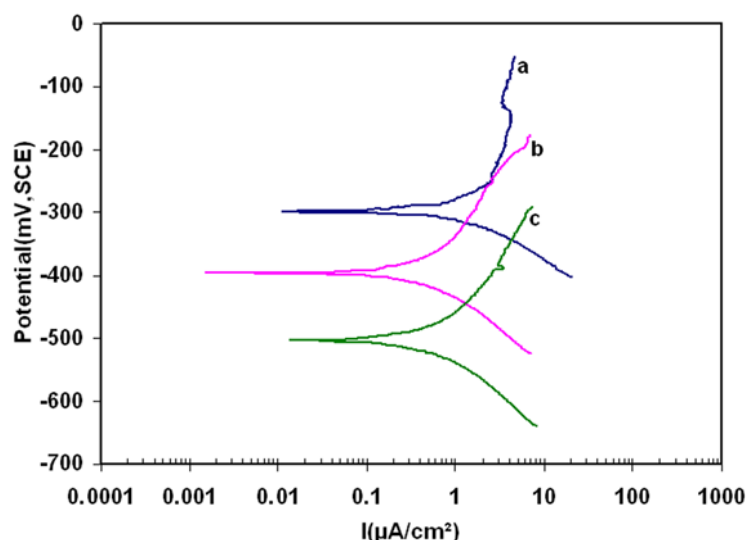


**Fig. 10.** The potentiodynamic polarization curves for: (a): the 316L stainless steel 316L electrode, and  $\text{TiO}_2$ -15% mol  $\text{SiO}_2$  film before (b): and after (c): UV illuminations in 3% wt NaCl solutions

properties. It has been found that the high acidic strength of  $\text{TiO}_2$ - $\text{SiO}_2$  composites is attributable to the acidity of Ti-O-Si bonds [31]. So, the composite surface can adsorb more hydroxyl radicals than the pure  $\text{TiO}_2$  surface [32]. Given the foregoing results, by adding  $\text{SiO}_2$  to  $\text{TiO}_2$  thin films the photoactivity of the composite should be better than that of pure  $\text{TiO}_2$ .

Fig. 10 shows the potentiodynamic polarization curves for the  $\text{TiO}_2$ - $\text{SiO}_2$  film which contained 15% mol of  $\text{SiO}_2$  before and after the UV illuminations and for a stainless steel 316L electrode in 3% wt NaCl solutions.

When the UV lamp was turned on, the OCP was shifted to  $-503$  mV (SCE) and the anodic polarization was dramatically facilitated. Higher photoactivity of silica-embedding titania compared with the pure  $\text{TiO}_2$  is brought about by higher heat treatment in the absence of rutile phase formation which results in the production of the anatase phase of high crystallinity and effectively reduces the bulk defects which serve as the recombination centers [24].

#### 4. Conclusion

1. In the present research, the thin films in which  $\text{SiO}_2$  was added to  $\text{TiO}_2$  were deposited on AISI 316L stainless steel, and the effect of the added amount of  $\text{SiO}_2$  on the films

morphology and its mechanical properties and corrosion behavior of 316L stainless steel substrate were studied.

2. It was observed that the addition of a proper amount of  $\text{SiO}_2$  to the  $\text{TiO}_2$  film not only caused the particle size of  $\text{TiO}_2$ - $\text{SiO}_2$  crystal to decrease but also could help improve the surface quality.

3. The minimum RMS value was obtained from the film with a silica content of 10% mol.

4. Mechanical and tribological properties of the films were improved in the range of 10–15% mol of  $\text{SiO}_2$  addition as compared to pure  $\text{TiO}_2$ .

5. By increasing the content of  $\text{SiO}_2$ , the minimum plastic index (Er/H ratio) and residual tensile strain were observed in the films with a silica content of 5 and 15 % mol, respectively.

6. The corrosion behavior of the 316L stainless steel was improved by adding 15% mol of  $\text{SiO}_2$  not only for irradiated film but also for the film that was kept in darkness.

7. Under the UV illumination conditions, photo-generated electrons were quickly accumulated in this film compared with the film kept in darkness resulting in more negative shift of the OCP of the film and thus the substrate was perfectly protected by the film photocathodically.

## References

1. G. X. Shen, Y. C. Chen and C. J. Lin, Corrosion protection of 316 L stainless steel by a TiO<sub>2</sub> nanoparticle coating prepared by sol-gel method, *Thin Solid Films*, Vol. 489, 2005, pp. 130.
2. M. Lia, S. Luo, P. Wu and J. Shen, Photocathodic protection effect of TiO<sub>2</sub> films for carbon steel in 3% NaCl solutions, *Electrochim. Acta*, Vol. 50, 2005, pp. 3401.
3. Z. Liu, Y. Dong, Z. Chu, Y. Yang, Y. Li and D. Yan, Corrosion behavior of plasma sprayed ceramic and metallic coatings on carbon steel in simulated seawater, *Mater. Design*, Vol. 52, 2013, pp. 630.
4. D. S. R. Krishna, Y. Sun and Z. Chen, Magnetron sputtered TiO<sub>2</sub> films on a stainless steel substrate: Selective rutile phase formation and its tribological and anti-corrosion performance, *Thin Solid Films*, Vol. 519, 2011, pp. 4860.
5. S. M. Madani, M. Ehteshamzadeh and H. H. Rafsanjani, Investigation of the microstructure and corrosion performance of a nanostructured titania-containing hybrid silicate film on mild steel, *Thin Solid Films*, Vol. 519, 2010, pp. 145.
6. T. K. Rout, N. Bandyopadhyay, R. Narayan, N. Rani and D. K. Sengupta, Performance of titania-silica composite coating on interstitial-free steel sheet, *Scripta Mater*, Vol. 58, 2008, pp. 473.
7. S. Vives and C. Meunier, Mixed SiO<sub>2</sub>-TiO<sub>2</sub> (1:1) sol-gel films on mild steel substrates: Sol composition and thermal treatment effects, *Surf. & Coat. Tech*, Vol. 202, 2008, pp. 2374.
8. T. Cetinkaya, L. Neuwirthová, K. Kutlákova, V. Tomásek and H. Akbulut, Synthesis of nanostructured TiO<sub>2</sub>/SiO<sub>2</sub> as an effective photocatalyst for degradation of acid orange, *Appl. Surf. Sci*, Vol. 279, 2013, pp. 384.
9. C. Beck, T. Mallat, T. Bürgi and A. Baiker, Nature of Active Sites in Sol-Gel TiO<sub>2</sub>-SiO<sub>2</sub> Epoxidation Catalysts, *J. Catal*, Vol. 204, 2001, pp. 428.
10. S. M. Jung, P. Grange, TiO<sub>2</sub>-SiO<sub>2</sub> mixed oxide modified with H<sub>2</sub>SO<sub>4</sub>: II. Acid properties and their SCR reactivity, *Appl. Catal. A-Gen*, Vol. 228, 2002, pp. 65.
11. J. Wang, C. Lua and J. Xiong, Self-cleaning and depollution of fiber reinforced cement materials modified by neutral TiO<sub>2</sub>/SiO<sub>2</sub> hydrosol photoactive coatings, *Appl. Surf. Sci.*, Vol. 298, 2014, pp. 19.
12. B. S. Boroujeny, A. Afshar v and A. Dolati, Photoactive and self-cleaning TiO<sub>2</sub>-SiO<sub>2</sub> thin films on 316L stainless steel, *Thin Solid Films*, Vol. 520, 2012, pp. 6355.
13. D. Zhu and T. Kosugi, Thermal conductivity of GeO<sub>2</sub>/SiO<sub>2</sub> and TiO<sub>2</sub>/SiO<sub>2</sub> mixed glasses, *J. Non-Cryst. Solids*, Vol. 202, 1996, pp. 88.
14. M. Aizawa, Y. Nosaka and N. Fujii, Preparation of TiO<sub>2</sub>/SiO<sub>2</sub> glass via sol-gel process containing a large amount of chlorine, *J. Non-Cryst. Solids*, Vol. 168, 1994, pp. 49.
15. X. Gao and I. E. Wachs, Titania-silica as catalysts: molecular structural characteristics and physico-chemical properties, *Catal. Today*, Vol. 51, 1999, pp. 233.
16. M. Fini, N. N. Aldini, P. Torricelli, G. Giavaresi, V. Borsari, H. Lenger, J. Bernauer, R. Giardino, R. Chiesa and A. Cigada, A new austenitic stainless steel with negligible nickel content: an in vitro and in vivo comparative investigation, *Biomaterials*, Vol. 24, 2003, pp. 4929.
17. J. A. Disegi and L. Eschbach, Stainless steel in bone surgery, *Injury*, Vol. 31, 2000, pp. D2.
18. Fujishima, T. N. Rao and D. A. Tryk, Titanium dioxide photocatalysis, *J. Photochem. Photobiol. C*, Vol. 1, 2000, pp. 1.
19. G. Lassaletta, A. Fernandez, J. P. Espinos, A.R. Gonzalez, Spectroscopic characterization of quantum-sized TiO<sub>2</sub> supported on silica: influence of size and TiO<sub>2</sub>-SiO<sub>2</sub> interface composition, *J. Phys. Chem*, Vol. 99, 1995, pp. 1484.
20. J. A. Mejias, V. M. Jimenez, G. Lassaletta, A. Fernandez, J. P. Espinos and A. R. Gonzalez, Interpretation of the Binding Energy and Auger Parameter Shifts Found by XPS for TiO<sub>2</sub> Supported on Different Surfaces, *J. Phys. Chem*, Vol. 100, 1996, pp. 16255.
21. W. C. Oliver and G. M. Pharr, An improved technique for determining hardness and elastic modulus using load and displacement sensing indentation experiments, *J. Mater. Res*, Vol. 7, 1992, pp. 1564.
22. H. Tang, F. Levy, H. Berger and P. E. Schmid, Urbach tail of anatase TiO<sub>2</sub>, *Phys. Rev*, Vol. 52, 1995, pp. 7771.
23. B. D. Cullity, *Elements of X-ray Diffraction*, Wesley Pub, Note Dame, 1978.
24. K. Y. Jung and S. B. Park, Anatase-phase titania: preparation by embedding silica and photocatalytic activity for the decomposition of trichloroethylene, *J. Photochem. Photobiol. A: Chem*, Vol. 127, 1999, pp. 117.
25. G. Xu, Z. Zheng, Y. Wu and N. Feng, Effect of silica on the microstructure and photocatalytic properties of titania, *Ceram. Int.*, Vol. 35, 2009, pp. 1.

- 26.
27. M. Machida, K. Norimoto, T. Watanabe, K. Hashimoto and A. Fujishima, The effect of SiO<sub>2</sub> addition in super-hydrophilic property of TiO<sub>2</sub> photocatalyst, *J. Mater. Sci*, Vol. 34, 1999, pp. 2569.
28. H. Dong and T. Bell, Designer surfaces for titanium components, *Anti-Corros. Method M*, Vol. 46, 1999, pp. 338.
29. Leyland and A. Matthews, On the significance of the H/E ratio in wear control: a nanocomposite coating approach to optimised tribological behavior, *Wear*, Vol. 246, 2000, pp. 1.
30. P. Evans, T. English, D. Hammond, M. E. Pemble and D. W. Sheel, The role of SiO<sub>2</sub> barrier layers in determining the structure and photocatalytic activity of TiO<sub>2</sub> films deposited on stainless steel, *Appl. Catal. A-Gen*, Vol. 321, 2007, pp. 140.
31. L. Bamoulid, F. Benoît-Marquié, L. Aries, A. Guenbour, A. B. Bachir, M. T. Maurette, F. Ansart and S. El Hajjaji, Investigations on composition and morphology of electrochemical conversion layer/titanium dioxide deposit on stainless steel, *Surf. & Coat. Tech*, Vol. 201, 2006, pp. 2791.
32. M. Itoh, H. Hattori and K. Tanabe, The acidic properties of TiO<sub>2</sub>-SiO<sub>2</sub> and its catalytic activities for the amination of phenol, the hydration of ethylene and the isomerization of butane, *J. Catal*, Vol. 35, 1974, pp. 225.
33. M. Zhang, L. Shi, S. Yuan, Y. Zhao and J. Fang, Synthesis and photocatalytic properties of highly stable and neutral TiO<sub>2</sub>/SiO<sub>2</sub> hydrosol, *J. Colloid Interface Sci*, Vol. 330, 2009, pp. 113.